

Supplementary Figure Legends

Figure S1. A preparation of purified human proteasomes that lack endogenous Usp14, but contain Uch37. **a, b,** Human proteasomes were affinity-purified from an hRpn11-tagged line of HEK293T cells¹ as described in Supplementary Methods. Indicated amounts of proteasomes were analyzed by SDS-PAGE and immunoblotted with anti-Usp14 antibody. Samples were compared to recombinant Usp14 protein and lysates from wild-type and *usp14*^{-/-} MEFs. Lanes 1 and 2 of panel b were loaded with 0.6 pmol of proteasome. **c,** Nondenaturing gel analysis of purified human proteasomes (7 μ g) pre-treated with Ub-VS (+VS) or untreated (-VS) with suc-LLVY-AMC staining. **d,** One dimensional SDS-PAGE and Coomassie Brilliant Blue (CBB) staining of human proteasomes (6 μ g). This, together with **c**, suggests that there is essentially no change in proteasome integrity upon Ub-VS treatment of human proteasomes. **e,** Immunoblot analysis with anti-Uch37 antibody demonstrates the presence of endogenous Uch37 in the purified proteasomes (1.5 μ g). Reactivity with Ub-VS indicates that the band represents active Uch37. Asterisks (*) indicate nonspecific signals. Note that, in a separate experiment, the stoichiometry of Uch37 on proteasomes purified from tagged HEK293 cells was estimated using purified, recombinant Uch37 as a standard. This visual assay allowed for a rough estimate of one Uch37 molecule to one proteasome (data not shown).

Figure S2. Reconstitution of Usp14-proteasome complexes. **a,** CBB staining of purified recombinant proteins (0.5 μ g protein/lane). **b,** Gel-shift assay of Usp14-

proteasome binding. Purified human proteasomes (1 pmol per reaction) were incubated for 20 min at 30°C with 5 pmol of GST, GST-Usp14-wt, GST-Usp14-CA, untagged Usp14-wt, or untagged Usp14-CA. Samples were resolved by nondenaturing PAGE and proteasomes visualized by suc-LLVY-AMC in-gel hydrolysis. Binding of GST-Usp14 to proteasomes significantly reduced their electrophoretic mobility. Bottom, CBB staining of the gel after gel-shift assay. **c**, Ub-VS labeling of recombinant Usp14. 11 nM of recombinant Usp14 was incubated with 110 nM of VS-Ptsm in the absence or presence of Ub-VS (1 μ M) at 30°C for 1 hr. Samples were analyzed by SDS-PAGE/immunoblot. The result is a representative of two comparable experiments. This experiment shows that the bulk of recombinant Usp14 is Ub-VS modifiable and thus functionally intact.

Figure S3. Kinetic analysis of reconstituted Usp14-proteasome complexes. **a**, Linear kinetics ($R^2 > 0.99$) of the initial rates of Ub-AMC (1 μ M) hydrolysis by Usp14 and proteasome (1 nM). **b**, Michaelis-Menten plot of Usp14-dependent Ub-AMC (1 μ M) hydrolysis in the presence of human proteasome (1 nM) for 25 min. The data were fit to a hyperbolic curve by nonlinear regression ($R^2 > 0.99$). Approximate K_d and k_{cat} were determined as 4.0 ± 0.5 nM and $(22 \pm 0.4) \times 10^{-2} \text{ sec}^{-1}$, respectively. **c**, Linear kinetics ($R^2 > 0.99$) of Ub-AMC hydrolysis at 4 nM Usp14 and 1 nM proteasome. **d**, Michaelis-Menten plot of concentration-dependent Ub-AMC cleavage in the presence of Usp14 (4 nM) and proteasome (1 nM) for 30 min. The data are fit to a hyperbolic curve by nonlinear regression ($R^2 > 0.99$). Approximate K_M and k_{cat} were determined as 11 ± 2.7 μ M and $(53 \pm 7.1) \times 10^{-2} \text{ sec}^{-1}$, respectively. The graphs shown are representative of at

least three independent determinations and each data point is the mean \pm SD of triplicate determinations.

Figure S4. Usp14 does not regulate mRNA encoding Tau or TDP-43. *Usp14*^{-/-} MEFs were cotransfected with plasmids expressing Tau (**a**) or TDP-43 (**b**) and Usp14 wild-type or a mutant. Control indicates pcDNA3 empty vector cotransfection. After 2 days, total RNA was isolated through Trizol extraction and further purified using an RNeasy column. Quantitative RT-PCR was performed using primers for Tau (Forward: AAGGTGACCTCCAAGTGTGG, Reverse: GGGACGTGGGTGATATTGTC) and TDP-43 (Forward: ATGGAAAACAACCGAACAGG, Reverse: CAGTCACACCATCGTCCATC). mRNA levels were normalized to that of the GAPDH gene (Forward: GAGTCAACGGATTTGGTCGT, Reverse: GACAAGCTTCCCGTTCTCAG). The values plotted are means \pm SD of three independent experiments.

Figure S5. Stabilization of Tau by wild-type Usp14. *Usp14*^{-/-} MEFs were cotransfected with a plasmid expressing Tau and a plasmid expressing either wild-type Usp14 or its catalytically inactive mutant Usp14-CA. Chase experiments (**a**) and quantification (**b**) were carried out at indicated time points after the addition of 75 μ g/mL cycloheximide at time zero. The chase was initiated 36 hrs after transfection. Anti-Tau and anti-actin antibodies were simultaneously incubated for immunoblot. For each time point, the Tau signal was normalized to that of endogenous actin. Band intensities were quantified using Odyssey software ver. 3.0 from three independent experiments (n=3).

Note that Tau levels were reduced in the mutant already at time zero (to 67% of wild-type), presumably as a result of elevated Tau degradation prior to cycloheximide addition. This effect is normalized out in panel b.

Figure S6. Usp14-SF does not significantly stabilize Arg-GFP in *usp14*^{-/-} MEF cells. An N-end rule substrate, Arg-GFP, is responsive to the Usp14 noncatalytic effect as shown in **Fig. 1f**. Arg-GFP (3 μg plasmid DNA transfected per sample) was coexpressed with either wild-type Usp14 (Usp14-wt), catalytically inactive Usp14-CA (Usp14-CA), or a naturally occurring splice variant, the short form of Usp14 (Usp14-SF) (2 μg DNA /sample) in *usp14*^{-/-} MEFs. Protein extracts were prepared two days after transfection, and analyzed by SDS-PAGE and anti-GFP immunoblot as in **Fig. 1f**.

Figure S7. Primary screening of small-molecule libraries for Usp14 inhibition. Statistical plot of high-throughput compound screening. 63,052 compounds were screened in duplicate for inhibition of Usp14 (15 nM) in the presence of proteasome (1 nM). A 384-well, low volume (20 μl) plate format was used. Data processing was done by a 'robust' Z-score method as previously described² and each compound was plotted using Spotfire software. The Z-score is a normalized value that takes into account plate-to-plate variation that would otherwise make it difficult to compare data from different plates across the screen. Here, weak hits are designated as $-3.5 > Z > -7$, medium hits as $-7 > Z > -10$, and strong hits as $Z < -10$. Compounds with a Z score less than -3.5 were selected for secondary screening. Compounds over the cut-off of $Z > 5$ are mostly autofluorescent molecules and were not plotted.

Figure S8. IU1, a Usp14 inhibitor, inhibits the catalytic activity of proteasome-associated Usp14 *in vitro*. **a**, IU1 is only weakly inhibitory towards proteasome-free Usp14. 2 μM of recombinant Usp14 protein in the absence of proteasome was treated with either IU1 or IU1C (17 μM). **b**, IU1 (17 μM) shows little inhibitory activity in Ub-AMC hydrolysis assays of human proteasomes not treated with Ub-V5. These data complement **Fig. 2c** and demonstrate that IU1 does not affect the DUB activity of proteasome-bound Uch37. **c**, **d**, Two independent IC_{50} curves of proteasome-associated Usp14 treated with IU1. Usp14 was preincubated with IU1 for either 45 min (Exp1) or 30 min (Exp2). The data were fit to a four parameter logistic model (the Hill-slope model) based on guidelines from NIH Chemical Genomics Center (http://ncgc.nih.gov/guidance/manual_toc.html). Error bars indicate SDs (n=3). Note that, in related experiments, IU1 was shown not to be a fluorescent quencher for AMC (data not shown). See **Supplementary Methods** for the detailed assay conditions.

Figure S9. The specificity of IU1 for Usp14 is observed independently of Ub-AMC concentration. Assays of Ub-AMC hydrolysis were done as in **Fig. 2c**, except lower concentrations of Ub-AMC were used. Similar results were obtained for Usp2 (data not shown).

Figure S10. Summary of K_M values for Ub-AMC of deubiquitinating enzymes in this study. K_M values of DUBs used in the selectivity assays were obtained from the literature. Unknown K_M values were determined in this study, as indicated. These values

are significant because the DUB assays (of **Supplementary Fig. 9**) should be most sensitive to inhibition when substrate is at a low concentration as compared to the K_M of the enzyme in question.

Figure S11. Characterization of IU1C, an inactive variant of IU1. **a**, Dose-response curves for inhibition of various deubiquitinating enzymes by IU1C *versus* IU1. IU1 data are taken from **Fig. 2b**. **b**, Assays of deubiquitinating enzyme inhibition by IU1C. Compare to **Fig. 2c**. Conditions as in **Fig. 2c**. All values are presented as mean \pm s.d. (n=3). **c**, IU1C does not significantly affect Tau levels in wild-type MEF cells. Compare to **Fig. 4a**. Conditions as in **Fig. 4a** except no LacZ coexpression (i.e., IU1C was used at 0, 25, 50, 75, or 100 μ M in a 6-hr treatment).

Figure S12. IU1 does not interfere with Usp14 binding to human proteasomes. **a**, Human proteasomes (\sim 4 nM) were first collected, using NeutrAvidin agarose (Thermo Scientific), from \sim 2 mg of lysate from HEK293T cells harboring Rpn11-HTBH. After incubating with recombinant Usp14 (80 nM) in the presence or absence of the indicated compound, followed by washing with low salt lysis buffer, the association between Usp14 and the proteasome was determined by immunoblotting. The experiment was performed in duplicate and additionally repeated. **b**, as in **a**, except \sim 2-fold molar excess of Usp14 was incubated with the proteasome in the absence or presence of the indicated compound (30 μ M). The asterisk (*) denotes a nonspecific signal generated by the anti-Usp14 antibody.

Figure S13. Reversibility of Usp14 inhibition by IU1 after prolonged incubation. **a**, IU1 inhibits proteasome-associated Usp14 activity without a detectable lag period. 2.5 nM of human proteasome was mixed with 30 nM of recombinant Usp14 protein. The reaction was then initiated by adding 1 μ M Ub-AMC. After 30 min, IU1 (100 μ M) or vehicle (DMSO) was added to the sample. **b**, These data complement **Fig. 2d**. 60 nM of Usp14 and 5 nM human proteasome were treated with vehicle or 100 μ M of IU1 for 2 hr. The sample was then subjected to three rounds of ultrafiltration, using a Microcon-YM3 filter (3 kDa cutoff, Millipore). After each spin, the protein complex was resuspended to the original volume and assayed for DUB activity. **c**, The DUB activity of Usp14 is stable in the presence of human proteasome for at least 8 hrs. **d**, As in **Fig. 2d** except prolonged incubation (5 and 8 hr) was tested and the percent DUB activity was normalized to 26S peptidase activity (i.e. LLVY-AMC hydrolysis). IU1 was added to 100 μ M. **e**, Immunoblot analysis showing that there are essentially no changes of protein level after multiple rounds of sample concentration using Microcon-YM3 filters. There is some protein loss after gel filtration by Centriscin-10, but the amount of protein is comparable between IU1 treated and nontreated samples. SDS-PAGE/immunoblot was done with the same samples as used in **Fig. 2d** and **Supplementary Fig. 13b**.

Figure S14. Chain trimming assays with human proteasome and RP purified in the presence of ADP. **a**, **b**, Nondenaturing gels (**a**) and SDS-PAGE gel analysis (**b**) of purified human proteasomes with ATP (ATP prep) or ADP (ADP prep). 7 μ g was used for nondenaturing gel analysis and 6 μ g for SDS-PAGE. Note that the ADP sample contains a mixture of proteasome 26S holoenzyme and 19S RP, due to CP-RP

dissociation during purification (see also ref 3). **c**, Ub-AMC and LLVY-AMC hydrolysis assays. **d**, *In vitro* Ub_n-ClnB degradation assays with samples prepared and assayed in the presence of ATP or ADP. Samples were analyzed by SDS-PAGE/immunoblotting. These data complement **Fig. 3a**. **e**, *In vitro* Ub_n-ClnB chain trimming assays with samples prepared and assayed in the presence of ADP. IU1 is effective at inhibition of chain trimming at approximately 5 μM, as expected from Ub-AMC hydrolysis data.

Figure S15. IU1 does not affect cyclin B degradation in the presence of Usp14-CA.

Assays were done as in **Figs. 1b** and **3b**.

Figure S16. Chemical analysis of IU1 and IU1C. **a, b**, ¹H-NMR spectroscopic data of IU1 (**a**) and IU1C (**b**). LC/MS analysis using IU1 (**c**) and IU1C (**d**). TIC, total ion count. SPC, shared peak count extracted from the peak with retention time 15 min (IU1) or 23 min (IU1C). Additional information is available in **Supplementary Methods**.

Figure S17. IU1 uptake into cells measured by LC/MS. **a**, Standardization of LC/MS for IU1 detection. Ion count LC/MS traces (*m/z* at 301) of various concentrations of IU1. Cell-associated IU1 was monitored using an Agilent series 1200 LC/6130 system with a reversed-phase C₁₈ column. The retention time for IU1 is ~8.8 min. **b**, Ion count peak areas *versus* concentration of IU1. The LC/MS shows linear responses in the given range of concentration ($R^2=0.99$). **c**, Wild-type MEFs were treated with 50 μM of IU1 for various times as indicated. Cell lysates were collected, extracted with ethyl acetate, and subjected to mass spectrometry (see details in **Supplementary Methods**). Ion counts of

LC/MS traces (m/z at 301) at 0 hr, 1 hr, 24 hr, and an IU1 standard solution at 1 $\mu\text{g/mL}$, are shown. ns, nonspecific.

Figure S18. Entry of IU1 into wild-type MEF cells monitored by HPLC with UV detection. **a**, The UV spectrum of IU1. IU1 shows absorption maxima at 255 nm and 305 nm. **b**, HPLC chromatograms showing the time-dependence of IU1 internalization at 300 nm. Cell lysates were processed as described in the legend to **Supplementary Fig. 17**. The standard shows results obtained using purified IU1 at 1 $\mu\text{g/mL}$. It is assumed that the retention of IU1 with the cell fraction reflects IU1 internalization.

Figure S19. Time-course of IU1 levels in cells and media. **a, b**, The IU1 concentration in wild-type MEF cells and 293 cells, determined by LC/MS. IU1 was added to cultures at 50 μM at time zero. ND, not detected. Similar results were obtained in *usp14*^{-/-} MEF cells. **c**, Internalized IU1 was rapidly released from cells. After wild-type MEFs were incubated with 50 μM of IU1 for one hour, the culture media were replaced with fresh media without IU1. Internalized IU1 was monitored at the indicated times. **d, e**, IU1 concentration in the media of HEK293 cells and *usp14*^{-/-} MEF cells. The comparable concentrations of IU1 from 1 hr to 48 hr indicate its stability in serum-containing media.

Figure S20. Assessment of IU1 cytotoxicity in MEF cells, using the MTT assay. IU1 was added at various concentrations (12.5 μM to 1.5 mM) to +/+ (red squares) or *usp14*^{-/-} MEFs (blue triangles). After the indicated incubation times, 25 μL of a 5 mg/mL

MTT solution was added to sample and the plates were incubated for 2 hr at 37°C. The MTT-formazan crystals that had formed were dissolved by adding 200 μ L DMSO and the absorbance was measured at 550 nm. Each data point is a mean \pm SD of three independent experiments.

Figure S21. IU1 cytotoxicity assayed in MEF, 293, and HeLa cells. a-c, See legend to **Supplementary Fig. 20. d, e**, Live-cell imaging of IU1 effects on proliferation of Usp14 MEFs. Wild-type (**d**) or *usp14*^{-/-} (**e**) MEFs were plated into each well of a 24-well plate at 35,000 cells/well. On the following day, IU1 or vehicle was added, as indicated. Live cell proliferation was monitored over 72 hrs using an automated imaging system. Data points are means of duplicate measurements. **f**, Live-cell imaging of IU1 effects on HeLa cell proliferation.

Figure S22. IU1 does not induce apoptosis in wild-type MEF cells. Cells were treated with 100 μ g/mL of IU1 or DMSO control for 6 hr and a fluorescent TUNEL assay was performed with DAPI counterstaining. TUNEL-positive cells (arrow) were quantified and compared (right). Bars are the mean \pm s.e.m. of percentage of TUNEL positive cells from four independent experiments.

Figure S23. Quantitative analysis of Tau level after IU1 treatment in wild-type and *usp14*^{-/-} MEFs. a and b, As in **Figs. 4a** and **4b** except infrared dye-conjugated secondary antibodies were used for quantification using Odyssey imaging system. Tau signal intensities were normalized to that of endogenous actin and relative amounts are

shown. Primary antibodies were simultaneously incubated for immunoblot and band intensities were quantified using the Odyssey software.

Figure S24. IU1 reduces Tau and TDP-43 levels through a post-transcriptional effect. Tau (a) or TDP-43 (b) was transiently overexpressed in wild-type MEFs, which were then treated with IU1 as in **Figs. 4a** and **4e**, respectively. Total RNA was isolated and quantitative RT-PCR was performed as in **Supplementary Fig. 4**.

Figure S25. The stimulation of Tau degradation by IU1 is not mediated by autophagy. a, Transiently expressed mCherry-NBR1 levels in wild-type MEFs were significantly increased after treatment with 200 μ M of bafilomycin A₁ (BafA₁), an autolysosome formation inhibitor⁴, for 6 hr. b, Cells transfected with a plasmid expressing Tau were treated with 200 μ M of BafA₁ and/or 75 μ M of IU1 for 6 hrs, and analyzed by SDS-PAGE/immunoblot using the Odyssey infrared imaging system. c, Band intensities were quantified from three independent experiments (mean \pm SD) using Odyssey software.

Figure S26. IU1 treatment reduces the level of GFAP expressed in wild-type MEF cells but does not affect Arg-GFP. a, Wild-type MEF cells transfected with plasmids expressing wild-type GFAP or its more aggregation-prone mutations, GFAP-K63Q or GFAP-E210K were treated with 0, 25, 50, or 100 μ M of IU1 for 6 hr, and analyzed by SDS-PAGE/immunoblot. b, Lack of effect of IU1 on the degradation of Arg-GFP, which was stabilized by catalytically inactive Usp14-CA as in **Fig. 1f**. Otherwise short-lived

Arg-GFP was coexpressed with Usp14-CA in *usp14*^{-/-} MEF cells and treated with 0 - 100 μ M of IU1 for 6 hrs. Anti-GFP and anti-actin antibodies were used for immunoblotting. The noncatalytic effect of Usp14, which is best visualized in this assay, is not reversed by IU1.

Figure S27. Quantification of ubiquitin levels in Fig. 4g. Polyubiquitin and monoubiquitin levels from wild-type and *usp14*^{-/-} MEF were quantified after treatment of various concentration of IU1. Ub signals were normalized to that of endogenous actin. Quantification was achieved by densitometry of a film image.

Figure S28. IU1 treatment does not induce transcription of proteasome subunit genes. **a**, The level and peptidase activity of the proteasome were determined before and after a 6-hr IU1 treatment (100 μ M). Total cell extracts (50 μ g/lane) were resolved by native PAGE, and the proteasome was visualized using either an in-gel activity stain with a fluorogenic peptide substrate (LLVY-AMC), or immunoblotting with antibodies to subunit α 6. RP₂-CP and RP-CP are distinct forms of the 26S proteasome. **b**, A luciferase reporter gene containing the murine *Psmb5* promoter (-1 kb to 0 kb) was transiently expressed in wild-type and *usp14*^{-/-} MEFs and promoter activity was assessed following incubation of 25 or 50 μ M of IU1 for 8 hr. For normalization of luciferase activity, a control experiment using the promoter-less pGL3 plasmid was performed. This reporter construct has previously been used as a representative measure of proteasome subunit gene induction^{5,6}. Values are mean \pm SD from three independent experiments. RLU, relative light units. **c-e**, Quantitative RT-PCR for a

ubiquitin gene (UbB) and two proteasome subunit genes ($\alpha 5$ and $\alpha 7$) was performed using total mRNA from +/+ (left panels) and *usp14*^{-/-} MEFs (right) after incubation with a graded doses of IU1 for 6 hr. These data supplement **Fig. 4h**.

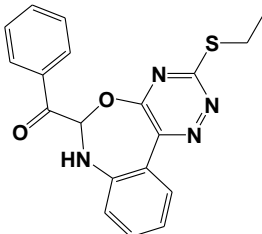
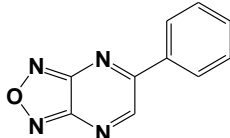
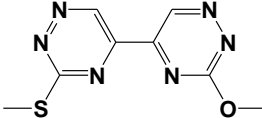
Figure S29. IU1C does not significantly affect oxidative stress-induced cytotoxicity. **a**, HEK293 cells were treated with 50 μ M of IU1C for 6 hr and graded concentrations of menadione for 4 hr, followed by MTT assay. Values represent the mean \pm SD of triplicate cultures. These data supplement **Fig. 5b**. Time-course of IU1C levels in wt MEFs (**b**) and HEK293 cells (**c**) were measure by using LC/MS. As in **Supplementary Figs. 19a** and **19b**, respectively, except IU1C, a functionally inactive control for IU1, was used. ND, not detected. **d and e**, See legend to **Supplementary Fig. 19c**. IU1C concentrations in the media (data not shown) of wild-type MEFs or HEK293 cells are comparable to those of IU1 (**Supplementary Fig. 19**).

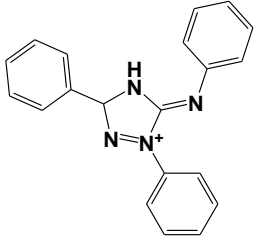
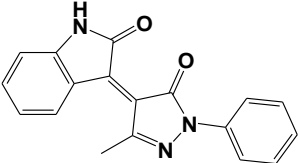
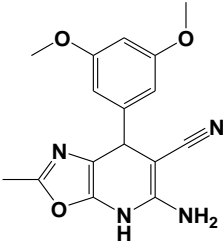
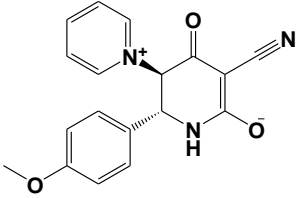
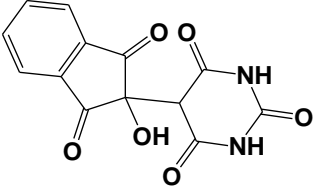
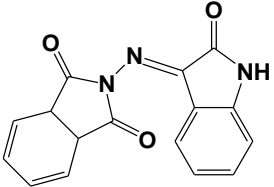
References accompanying supplementary figures

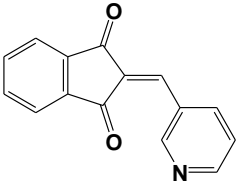
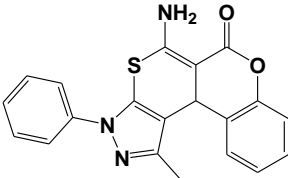
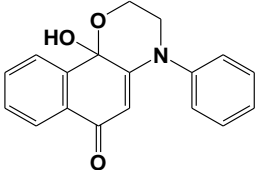
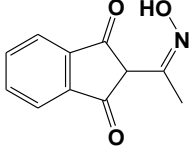
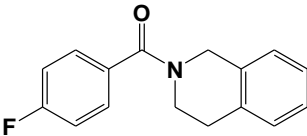
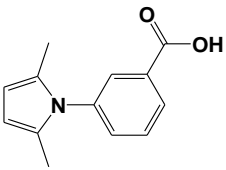
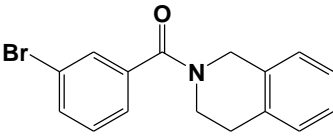
1. Wang, X. *et al.* Mass spectrometric characterization of the affinity-purified human 26S proteasome complex. *Biochemistry* **46**, 3553-65 (2007).
2. Malo, N., Hanley, J., Cerquozzi, S., Pelletier, J. & Nadon, R. Statistical practice in high-throughput screening data analysis. *Nat. Biotechnol.* **24**, 167-75 (2006).
3. Liu, C.W. *et al.* ATP binding and ATP hydrolysis play distinct roles in the function of the 26S proteasome. *Mol. Cell* **24**, 39-50 (2006).
4. Mizushima, N., Yoshimori, T., & Levine, B. Methods in mammalian autophagy research. *Cell* **140**, 313-26 (2010).
5. Kwak, M.K. *et al.* Antioxidants enhance mammalian proteasome expression through the Keap1-Nrf2 signaling pathway. *Mol. Cell. Biol.* **23**, 8786-94 (2003).
6. Chondrogianni, N. *et al.* Central role of the proteasome in senescence and survival of human fibroblasts. *J. Biol. Chem.* **278**, 28026-37 (2003).

Supplementary Table. Summary of nonspecific and weak hits

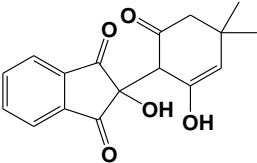
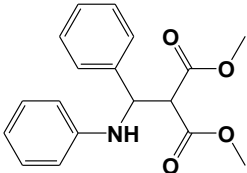
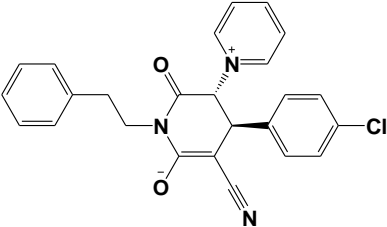
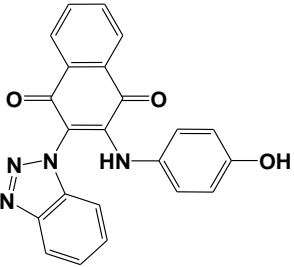
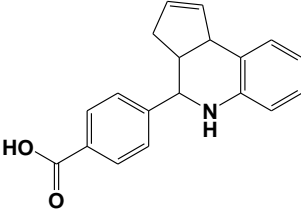
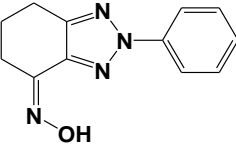
312 primary hits from high-throughput screening of the Ub-AMC hydrolyzing activity of Usp14 were tested for quenching of AMC amine as well as reproducible inhibition of proteasome-associated Usp14 activity in a dose- and time-dependent manner. Putative Usp14 inhibitors were then retested for their selectivity for Usp14 over IsoT. Inhibitors classified as nonspecific or weak are summarized below. Because their structures are unknown, nonspecific hits from a natural fungal extract library (MMV1) are not listed in the table. C1 to C191 indicates nonspecific hits and C'1 to C'9 weak hits. Note that, because initial hits from chemical screens are not always reproducible from fresh powder, the inhibitory species can in some cases be an impurity and, in particular, a breakdown product of that shown.

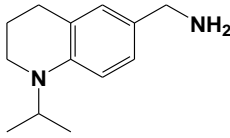
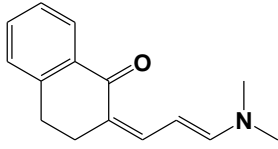
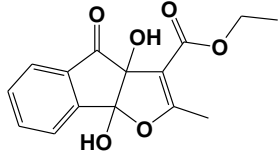
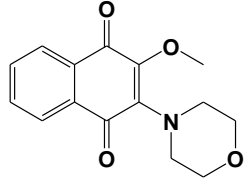
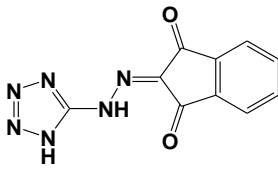
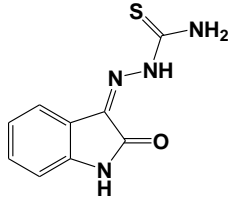
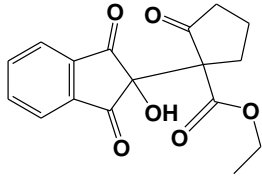
Name	Structure	Percent inhibition (at 17 μ M)	
		Usp14-26S	IsoT
C1		12	11
C2		8	7
C3		38	36

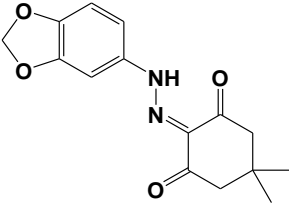
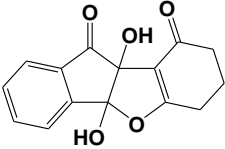
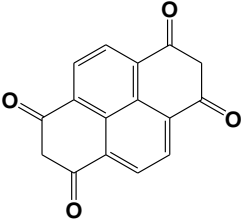
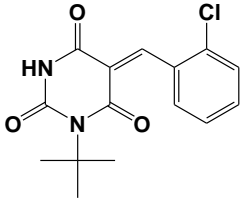
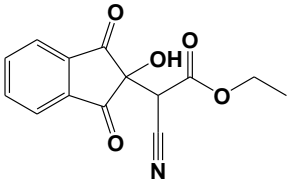
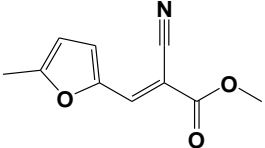
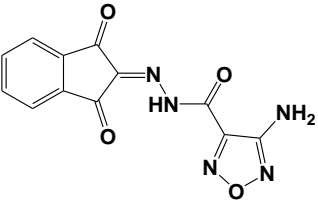
Name	Structure	Percent inhibition (at 17 μ M)	
		Usp14-26S	IsoT
C4		68	69
C5		92	95
C6		8	10
C7		48	76
C8		64	97
C9		50	71

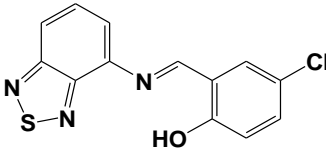
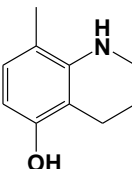
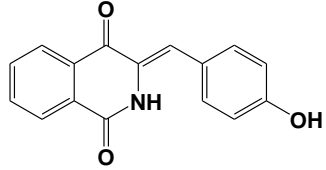
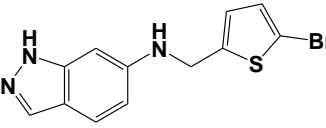
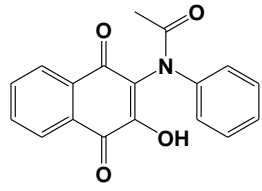
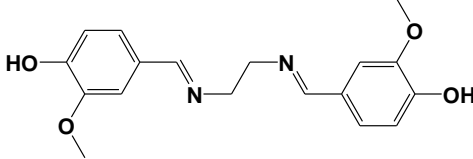
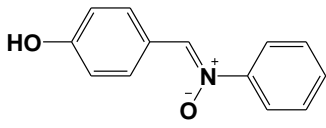
Name	Structure	Percent inhibition (at 17 μ M)	
		Usp14-26S	IsoT
C10		30	29
C11		22	60
C12		5	0
C13		34	27
C14		21	13
C15		49	43
C16		21	13

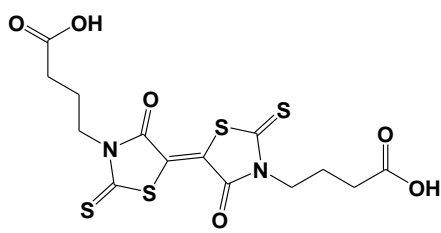
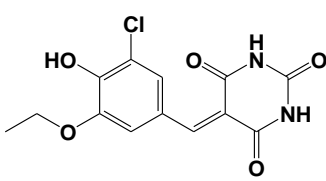
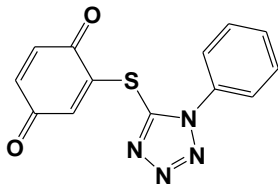
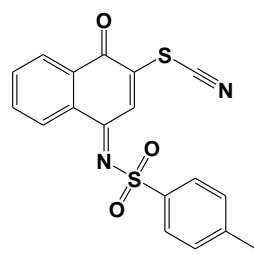
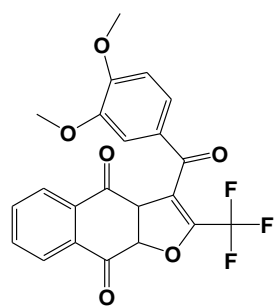
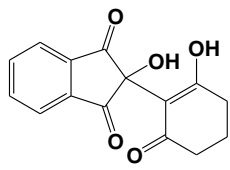
Name	Structure	Percent inhibition (at 17 μ M)	
		Usp14-26S	IsoT
C17		77	74
C18		11	8
C19		9	4
C20		23	45
C21		62	52
C22		28	66
C23		8	7

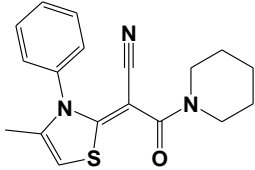
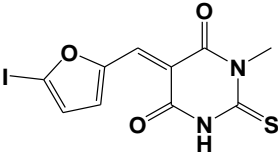
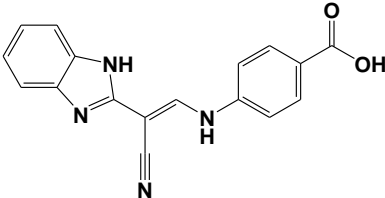
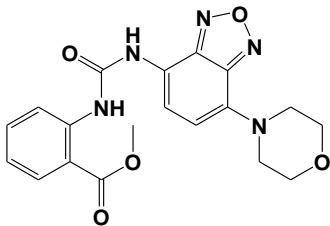
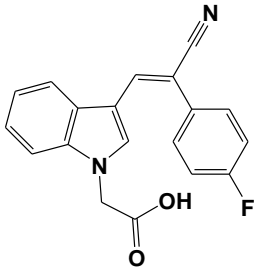
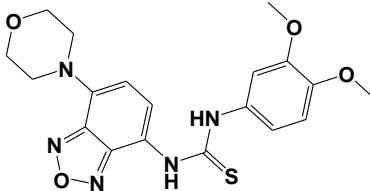
Name	Structure	Percent inhibition (at 17 μ M)	
		Usp14-26S	IsoT
C24		89	100
C25		39	58
C26		70	94
C27		80	96
C28		24	28
C29		80	96

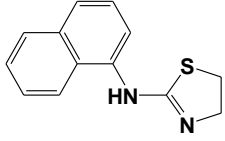
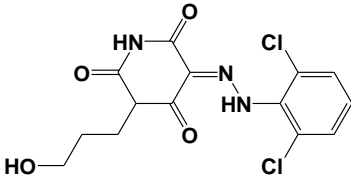
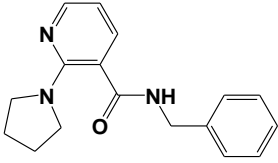
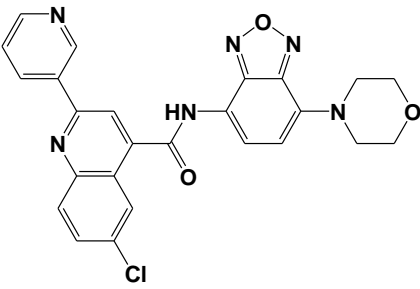
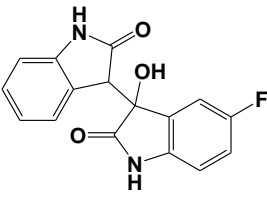
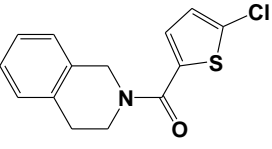
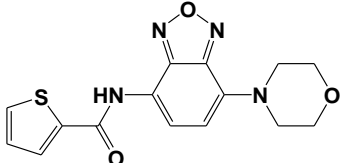
Name	Structure	Percent inhibition (at 17 μ M)	
		Usp14-26S	IsoT
C30		57	66
C31		70	84
C32		13	11
C33		22	16
C34		74	98
C35		8	7
C36		17	15

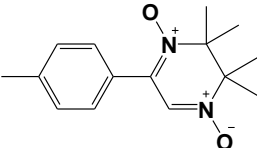
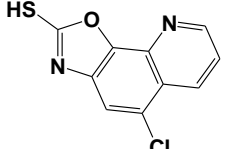
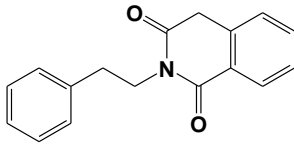
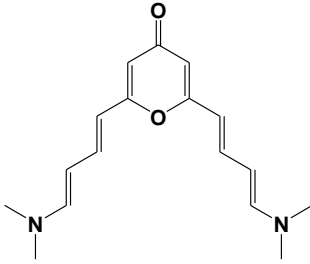
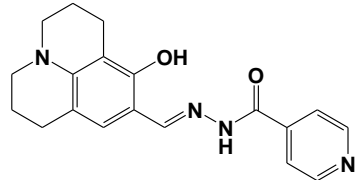
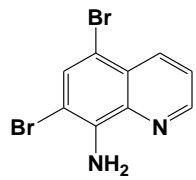
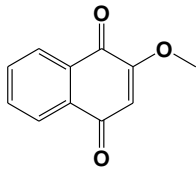
Name	Structure	Percent inhibition (at 17 μ M)	
		Usp14-26S	IsoT
C37		6	6
C38		79	97
C39		77	91
C40		30	27
C41		43	57
C42		12	10
C43		59	69

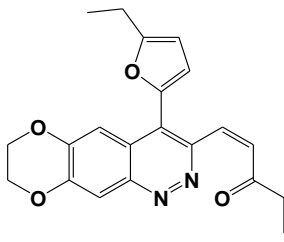
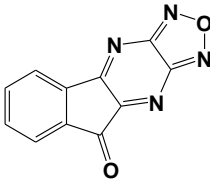
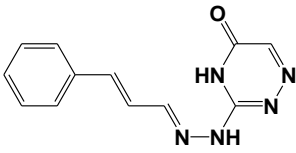
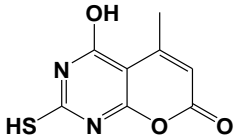
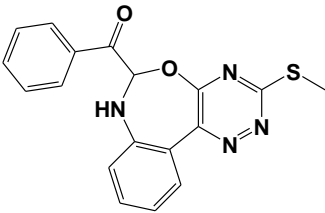
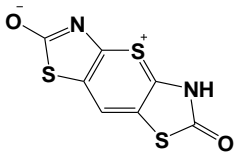
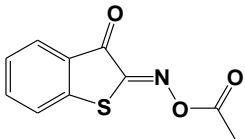
Name	Structure	Percent inhibition (at 17 μ M)	
		Usp14-26S	IsoT
C44		75	95
C45		55	61
C46		96	95
C47		75	95
C48		32	26
C49		16	11
C50		23	15

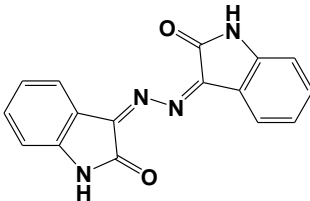
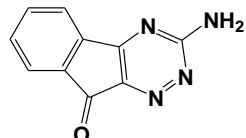
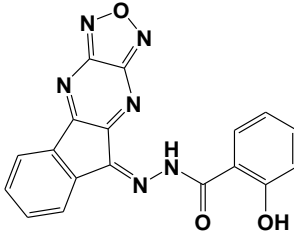
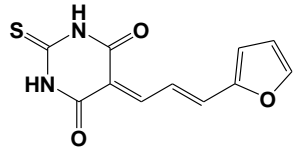
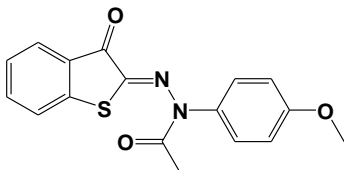
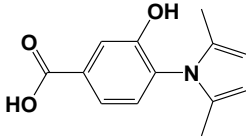
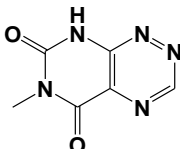
Name	Structure	Percent inhibition (at 17 μ M)	
		Usp14-26S	IsoT
C51		1	0
C52		35	34
C53		39	47
C54		93	90
C55		32	70
C56		81	84

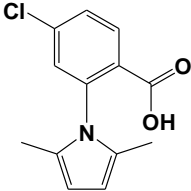
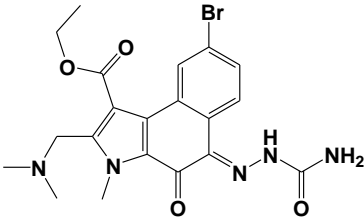
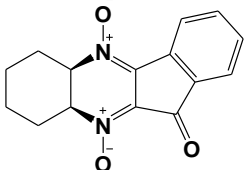
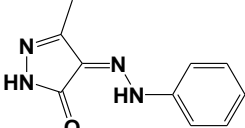
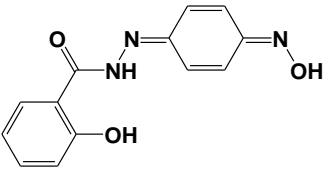
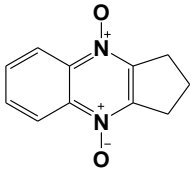
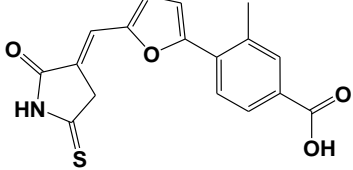
Name	Structure	Percent inhibition (at 17 μ M)	
		Usp14-26S	IsoT
C57		3	2
C58		36	34
C59		4	2
C60		51	51
C61		5	0
C62		92	96

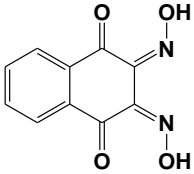
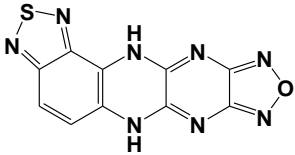
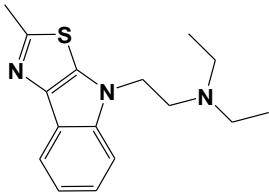
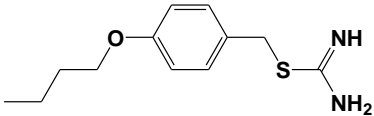
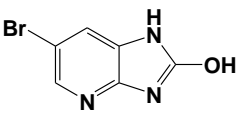
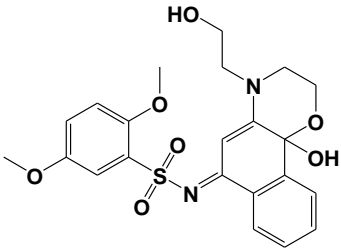
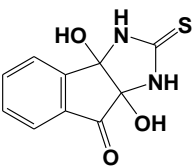
Name	Structure	Percent inhibition (at 17 μ M)	
		Usp14-26S	IsoT
C63		83	89
C64		28	28
C65		9	3
C66		69	93
C67		5	4
C68		22	21
C69		50	55

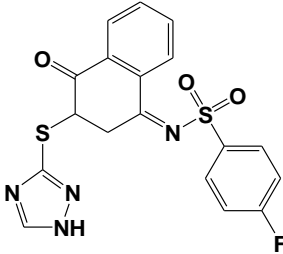
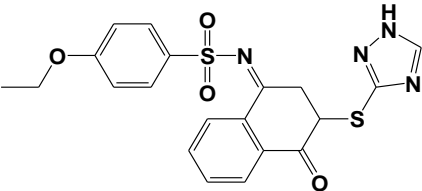
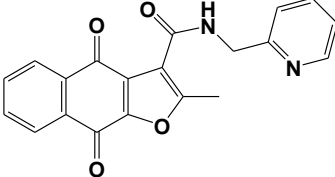
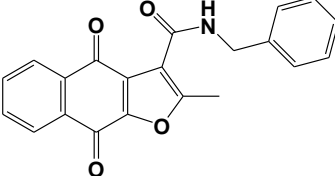
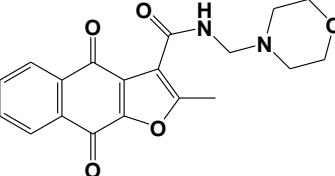
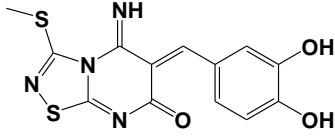
Name	Structure	Percent inhibition (at 17 μ M)	
		Usp14-26S	IsoT
C70		24	15
C71		51	85
C72		19	24
C73		3	1
C74		54	86
C75		65	81
C76		47	41

Name	Structure	Percent inhibition (at 17 μ M)	
		Usp14-26S	IsoT
C77		59	74
C78		31	31
C79		3	3
C80		16	6
C81		7	34
C82		4	3
C83		34	33

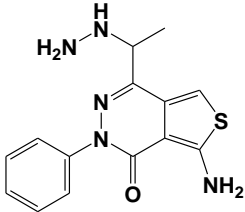
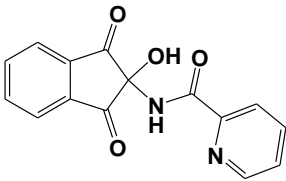
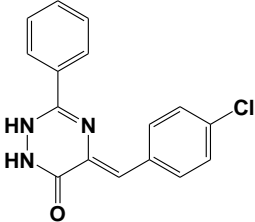
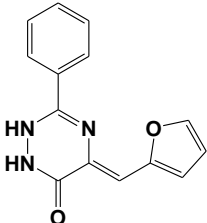
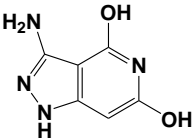
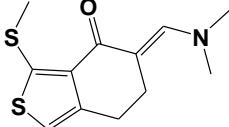
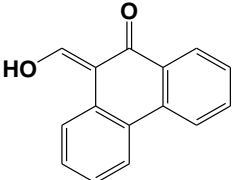
Name	Structure	Percent inhibition (at 17 μ M)	
		Usp14-26S	IsoT
C84		63	87
C85		60	62
C86		54	59
C87		36	45
C88		32	61
C89		39	19
C90		92	96

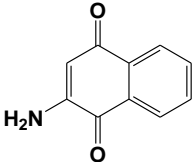
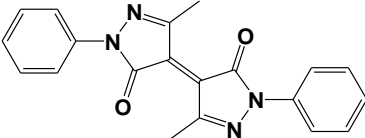
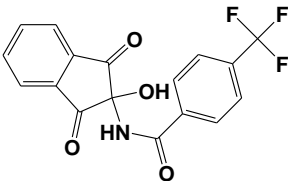
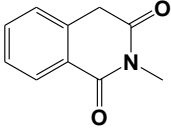
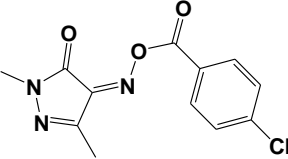
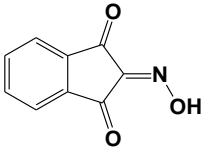
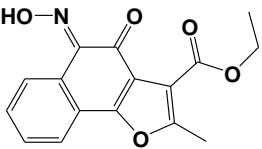
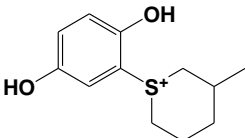
Name	Structure	Percent inhibition (at 17 μ M)	
		Usp14-26S	IsoT
C91		52	64
C92		88	80
C93		40	73
C94		26	21
C95		34	36
C96		26	21
C97		62	89

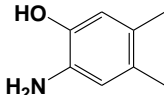
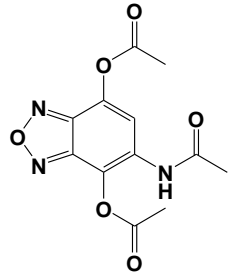
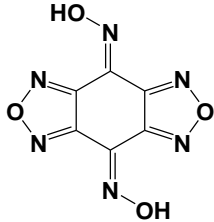
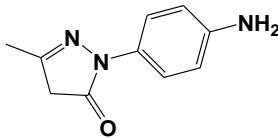
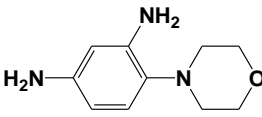
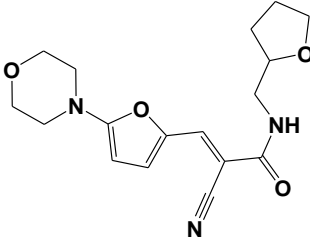
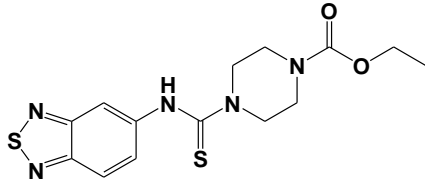
Name	Structure	Percent inhibition (at 17 μ M)	
		Usp14-26S	IsoT
C98		74	72
C99		78	93
C100		56	64
C101		4	3
C102		88	90
C103		69	75
C104		30	27

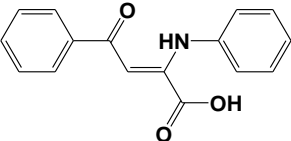
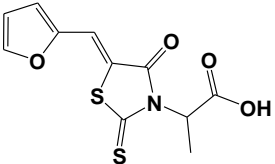
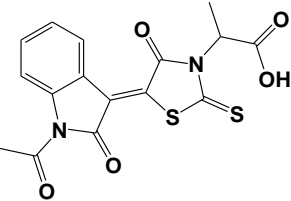
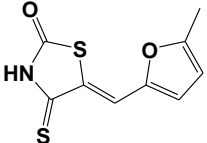
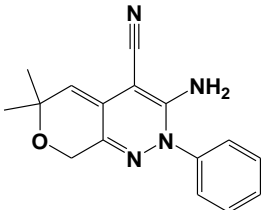
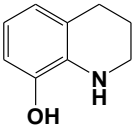
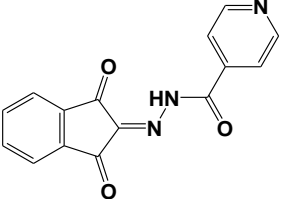
Name	Structure	Percent inhibition (at 17 μ M)	
		Usp14-26S	IsoT
C105		78	88
C106		81	84
C107		22	15
C108		34	27
C109		20	14
C110		6	6

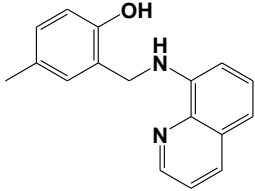
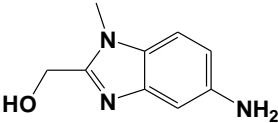
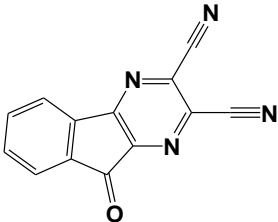
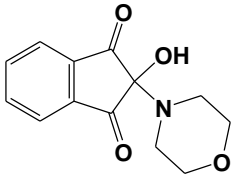
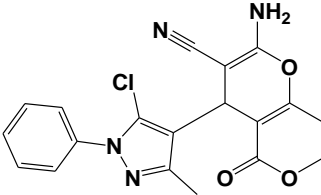
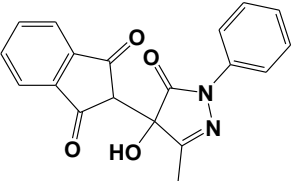
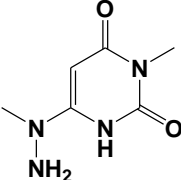
Name	Structure	Percent inhibition (at 17 μ M)	
		Usp14-26S	IsoT
C111		68	98
C112		53	76
C113		86	87
C114		92	96
C115		25	20
C116		83	85

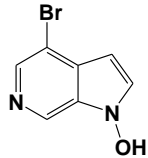
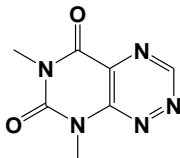
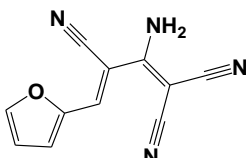
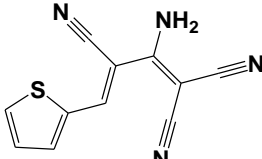
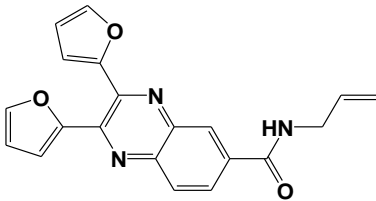
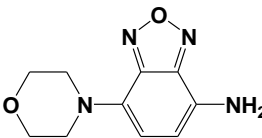
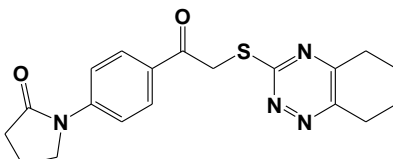
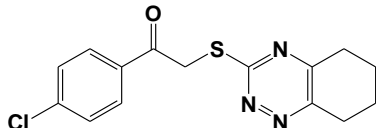
Name	Structure	Percent inhibition (at 17 μ M)	
		Usp14-26S	IsoT
C117		47	69
C118		20	24
C119		69	87
C120		49	49
C121		96	97
C122		82	68
C123		100	100

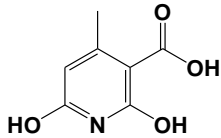
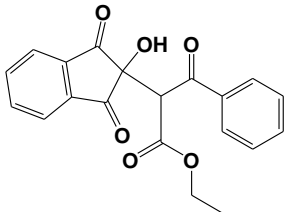
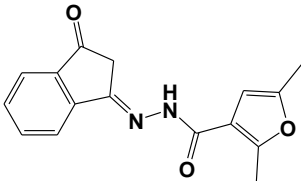
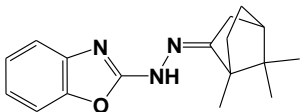
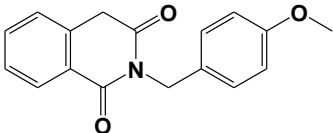
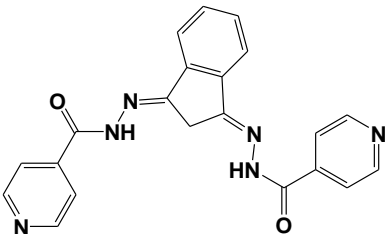
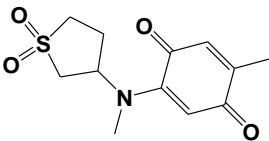
Name	Structure	Percent inhibition (at 17 μ M)	
		Usp14-26S	IsoT
C124		69	64
C125		93	100
C126		24	20
C127		23	21
C128		74	98
C129		84	94
C130		35	78
C131		81	91

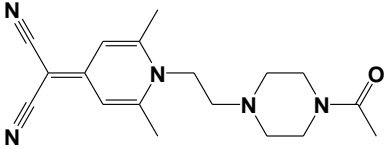
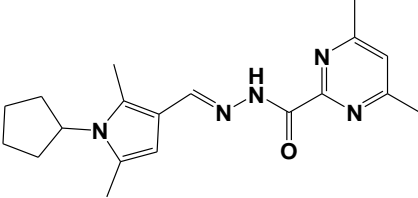
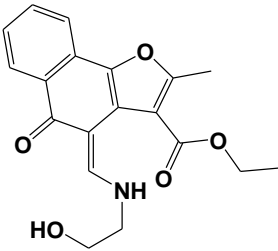
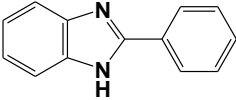
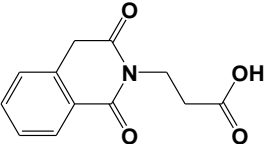
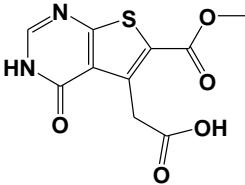
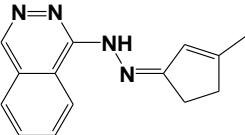
Name	Structure	Percent inhibition (at 17 μ M)	
		Usp14-26S	IsoT
C132		61	65
C133		64	70
C134		91	94
C135		91	97
C136		92	90
C137		17	18
C138		66	74

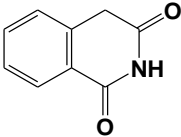
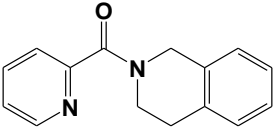
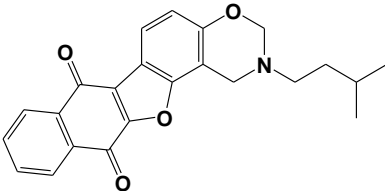
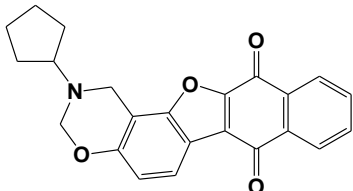
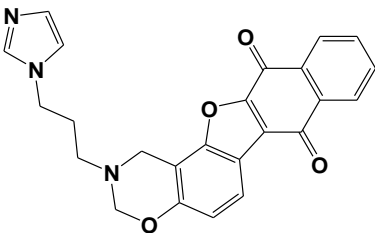
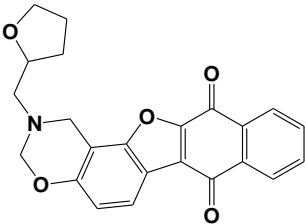
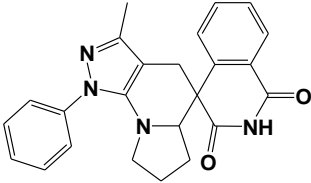
Name	Structure	Percent inhibition (at 17 μ M)	
		Usp14-26S	IsoT
C139		24	18
C140		17	15
C141		13	7
C142		73	83
C143		4	6
C144		39	44
C145		83	85

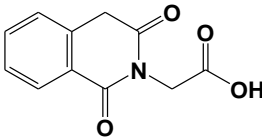
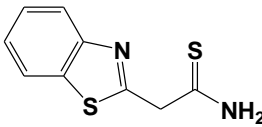
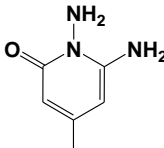
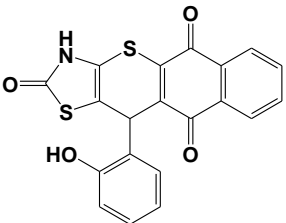
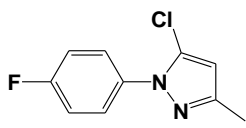
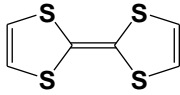
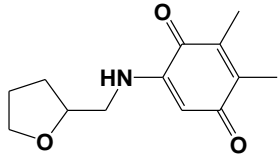
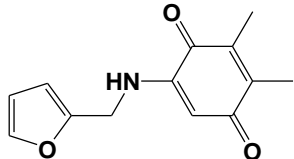
Name	Structure	Percent inhibition (at 17 μ M)	
		Usp14-26S	IsoT
C146		28	64
C147		62	62
C148		60	55
C149		59	54
C150		15	13
C151		6	7
C152		73	71

Name	Structure	Percent inhibition (at 17 μ M)	
		Usp14-26S	IsoT
C153		42	77
C154		96	98
C155		4	1
C156		12	6
C157		62	66
C158		93	94
C159		58	85
C160		52	49

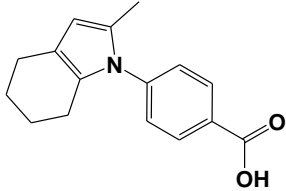
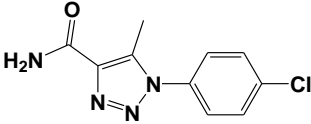
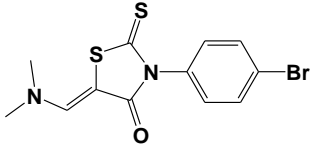
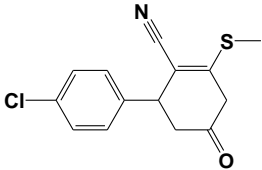
Name	Structure	Percent inhibition (at 17 μ M)	
		Usp14-26S	IsoT
C161		77	75
C162		48	70
C163		25	23
C164		32	28
C165		16	37
C166		94	96
C167		87	93

Name	Structure	Percent inhibition (at 17 μ M)	
		Usp14-26S	IsoT
C168		3	0
C169		77	81
C170		52	57
C171		30	26
C172		22	27
C173		43	44
C174		2	4

Name	Structure	Percent inhibition (at 17 μ M)	
		Usp14-26S	IsoT
C175		100	100
C176		33	59
C177		30	19
C178		43	38
C179		60	50
C180		58	52
C181		6	20

Name	Structure	Percent inhibition (at 17 μ M)	
		Usp14-26S	IsoT
C182		18	25
C183		30	29
C184		36	26
C185		62	56
C186		28	28
C187		54	54
C188		85	86
C189		44	39

Name	Structure	Percent inhibition (at 17 μ M)	
		Usp14-26S	IsoT
C190		3	3
C191		57	61
C'1		30	0
C'2		14	0
C'3		30	7
C'4		14	0
C'5		12	3

Name	Structure	Percent inhibition (at 17 μ M)	
		Usp14-26S	IsoT
C'6		11	0
C'7		33	2
C'8		27	0
C'9		10	1